

Strain Engineering 2D MoS₂ with Thin Film Stress Capping Layers

Tara Peña,^{*,†} Shoieb A. Chowdhury,[‡] Ahmad Azizimanesh,[†] Arfan Sewaket,[†]
Hesam Askari,[‡] and Stephen M. Wu^{†,¶}

[†]*Department of Electrical & Computer Engineering, University of Rochester, Rochester,
NY, USA.*

[‡]*Department of Mechanical Engineering, University of Rochester, Rochester, NY, USA.*

[¶]*Department of Physics & Astronomy, University of Rochester, Rochester, NY, USA.*

*E-mail: tpena@ur.rochester.edu

Abstract

In this work, we induce on-chip static strain into the transition metal dichalcogenide (TMDC) MoS₂ with e-beam evaporated stressed thin film multilayers. These thin film stressors are analogous to SiN_x based stressors utilized in CMOS technology. We choose optically transparent thin film stressors to allow us to probe the strain transferred into the MoS₂ with Raman spectroscopy. We combine thickness dependent analyses from Raman peak shifts in MoS₂ and atomistic simulations to understand the strain transferred throughout each layer. This collaboration between experimental and theoretical efforts allows us to conclude that strain is transferred from the stressor into the top few layers of MoS₂ and the bottom layer is always partially fixed to the substrate. This proof of concept suggests that commonly used industrial strain engineering techniques may be easily implemented with 2D materials, as long as the c-axis strain transfer is considered.

TMDCs have a multifaceted library of properties that can be altered with external perturbations, such as electric field effect, doping, etc.¹ Since these materials also exhibit high elastic limits, there exists an opportunity to use strain as another degree of freedom in engineering new nanoelectronic devices.² Strain engineered TMDCs may lead to a new generation of device structures that employ control over structural, electronic, optical, magnetic, superconducting, and topological materials' properties.³⁻⁷ Furthermore, on-chip straining techniques have already been well explored and implemented in semiconductor manufacturing, where strain is induced from lattice mismatched epitaxial growth and deposition of thin film stressors such as SiN_x.^{8,9} These techniques are well-characterized for 3D bonded materials, however there exists a gap to understand the implementation of these techniques onto 2D-bonded systems where the main feature is weak out-of-plane mechanical coupling.

There have been several approaches to strain TMDCs, specifically with fabricating suspended membrane structures, bending flexible substrates, and using diamond anvil cells.¹⁰⁻¹² While these approaches allow for precise control over strain, they are not ideal for on-chip applications since they require external macroscopic mechanical forces. In this Letter, we deposit e-beam evaporated optically transparent thin film stressors onto exfoliated MoS₂ to investigate the strain transferred into this 2D system. These stressors are polycrystalline thin films, which exhibit process induced stress similar to CVD grown SiN_x thin films. Almost all thin films possess process induced stress that results from its microstructural evolution during thin film growth.¹³ These thin film stressors are e-beam evaporated to minimize defect contribution in the TMDC samples.¹⁴ Deposition of magnesium fluoride (MgF₂) is well-known to provide tensile stress, while other materials such as magnesium oxide (MgO) and silicon dioxide (SiO₂) provide compressive stress.¹⁵⁻¹⁷ Figure 1a displays a visual representation of the samples, e-beam evaporated optically transparent thin film stressors deposited onto exfoliated MoS₂. For the case of depositing a tensile thin film stressor, the film

attempts to relax into a zero stress state by contracting. After depositing a tensile thin film stressor onto MoS₂, the stressor will contract and therefore lead to compressive strain transferred into the MoS₂ layers. Similarly with a compressive thin film stressor, the stressor will lead to tensile strain transferred into the MoS₂ layers.

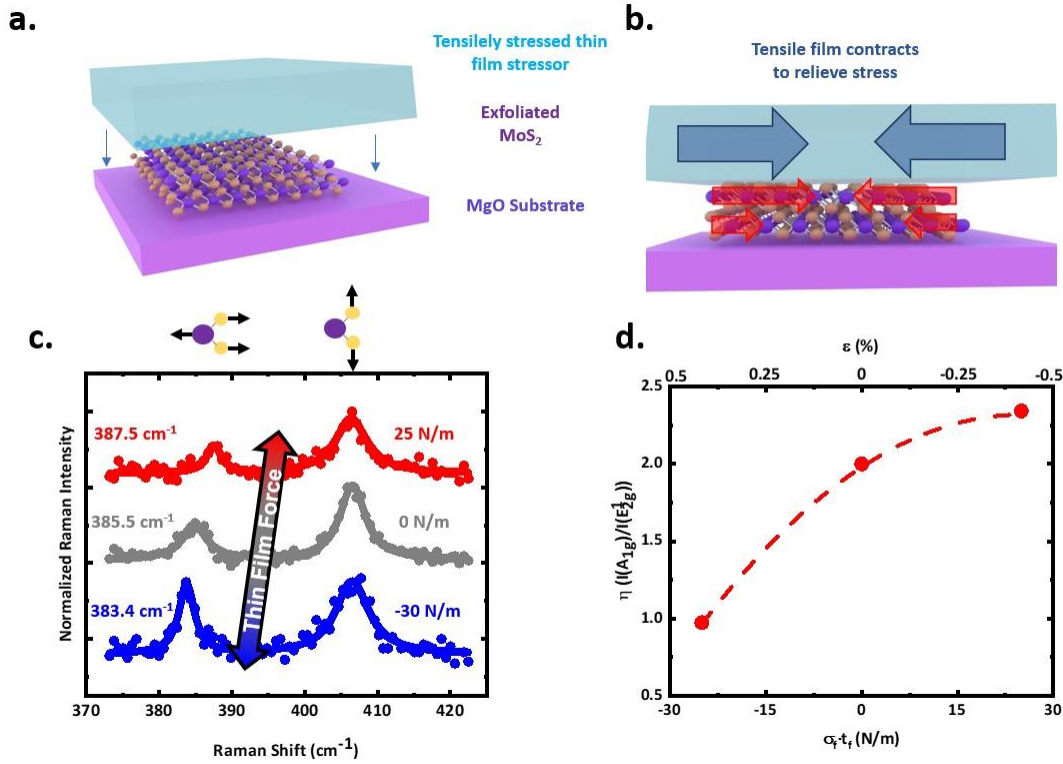


Figure 1: (a) Presentation of technique: MoS₂ is mechanically exfoliated onto a single-crystal MgO substrate, then a tensile optically transparent thin film stressor is evaporated on top. (b) The tensile thin film stressor will contract to release stress within itself, giving rise to compressively strained MoS₂. Strain transferred (red arrows) is presented to vary layer-by-layer. (c) Raman spectra of bilayer MoS₂ with a tensile thin film stressor (red), no thin film stressor (grey), and a compressive thin film stressor (blue). (d) Intensity of A_{1g} over the intensity of E_{2g}¹ versus thin film force and strain.

We choose MoS₂ as the base material, since the Raman modes with respect to strain and doping are well-characterized.¹⁸ The techniques we present here are equally applicable to any other 2D van der Waals bonded material. The exfoliated control MoS₂ layers are characterized via atomic force microscopy, Raman spectroscopy, and optical microscopy

(see Figure S1-S3).^{19,20} We focus on Raman peak shifts since the highest magnitude strain transmitted is 0.85%, therefore photoluminescence signatures are expected to be less than 100 meV (see Figure S4).¹⁰ MoS₂ flakes are exfoliated onto pre-polished single-crystal MgO substrates. The roughness of these substrates are confirmed to be 0.125 nm and below. We mitigate poor adhesion by annealing the substrates at 150 °C in a humidity-controlled environment (<1 ppm H₂O and O₂), limiting residual water and hydroxyl groups on the substrates' surface prior to TMDC exfoliation.²¹ Once exfoliation is completed, the samples are brought out of the glovebox and into an acetone, IPA ultrasound bath. The ultrasound bath allows for the poorly adhered flakes to be ripped from the substrate. The samples are then immediately placed into a vacuum chamber, where the thin film stressors are e-beam evaporated. The thin film stressors consist of three layers: an adhesive layer of 10 nm Al₂O₃, the stressor (MgF₂, MgO, or SiO₂) between 50 and 100 nm, then a final humidity protective layer of 10 nm Al₂O₃. Proper adhesion between each interface is essential for efficient strain transfer, therefore we choose an amorphous optically transparent thin film, Al₂O₃, to promote adhesion at the stressor and substrate interface. We observe negligible defects from deposition of the e-beam evaporated 10 nm adhesive Al₂O₃ layer by confirming that there are no changes in the Raman signature after deposition (Figure S5). The top 10 nm Al₂O₃ serves to protect the stressors from humidity, humidity is known to accelerate stress relaxation over time.²² All deposition processes began at 5×10^{-6} torr, with all growth rates kept between 1-2 Å/s. Cleaned glass slides are placed alongside of the samples during deposition. The radius of curvature of the glass slides are determined pre and post-deposition with a surface profilometer, which are used to determine thin film stress using the Stoney equation, the standard wafer curvature technique.²³

We then conduct Raman mapping on the samples of MoS₂ flakes with varying thin film forces (-30 N/m to +25 N/m). Thin film force is thin film stress times thin film thickness ($\sigma_f \cdot t_f$), this measurement is what quantifies the load being applied onto MoS₂ from the stressors.

Using a WITec Alpha300R Confocal Raman Microscope, we perform Raman mapping with 250 nm step size resolution. The 532 nm laser was focused on the sample using a 100x objective (0.90 N.A.), the spotsize of the laser is estimated to be $0.7 \mu\text{m}$. The power was monitored carefully to be 0.5 mW, to prevent sample damage from laser heating. Figure 1c

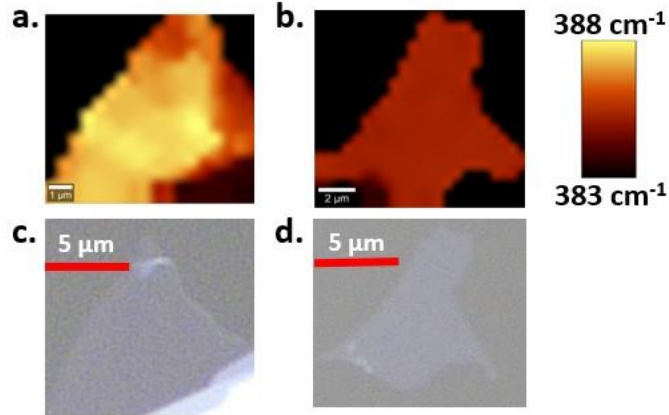


Figure 2: (a) E_{12g} peak position map of a 2L MoS_2 encapsulated with a tensile thin film MgF_2 stressor on a MgO substrate. (b) E_{12g} peak position map of a bare 2L MoS_2 on a MgO substrate. (c) Optical micrograph of the same encapsulated 2L MoS_2 . (d) Optical micrograph of the same control 2L MoS_2 .

presents Raman signatures from bilayer (2L) samples with varying thin film forces (presented above the Raman signatures on the right) extracted from the Raman mappings. Tensile MgF_2 films (red) create in-plane compressive strain throughout the MoS_2 samples, which is a result of the thin film stressor wanting to contract intrinsically to achieve a zero stress state. Similarly with compressive MgO and SiO_2 thin films (blue), stress relaxation of these thin films leads to transmitted in-plane tensile strain within the MoS_2 samples (Figure 1b,c). The control Raman signature (grey) is that of a 2L sample with no encapsulation. With application of thin film force onto the 2L MoS_2 samples, we measure shifts primarily within the E_{12g} modes and very little shifts in the A_{1g} mode as expected for in-plane strain. Figure 1d presents the Raman intensity ratio ($\eta = \frac{I(A_{1g})}{I(E_{2g}^1)}$) with applied thin film force and strain, this scaling trend matches theoretical predictions from biaxial strain.²⁴ The overall measured

Raman signatures are a superposition of Raman contributions from all layers within the given sample, therefore we will later couple these findings with results from atomistic models to extract the strain transmitted within each layer.

Figure 2a,b presents 2D Raman mappings of the E^{1}_{2g} modes from two 2L samples, an encapsulated and a control sample respectively. Figure 2a demonstrates a noticeably large

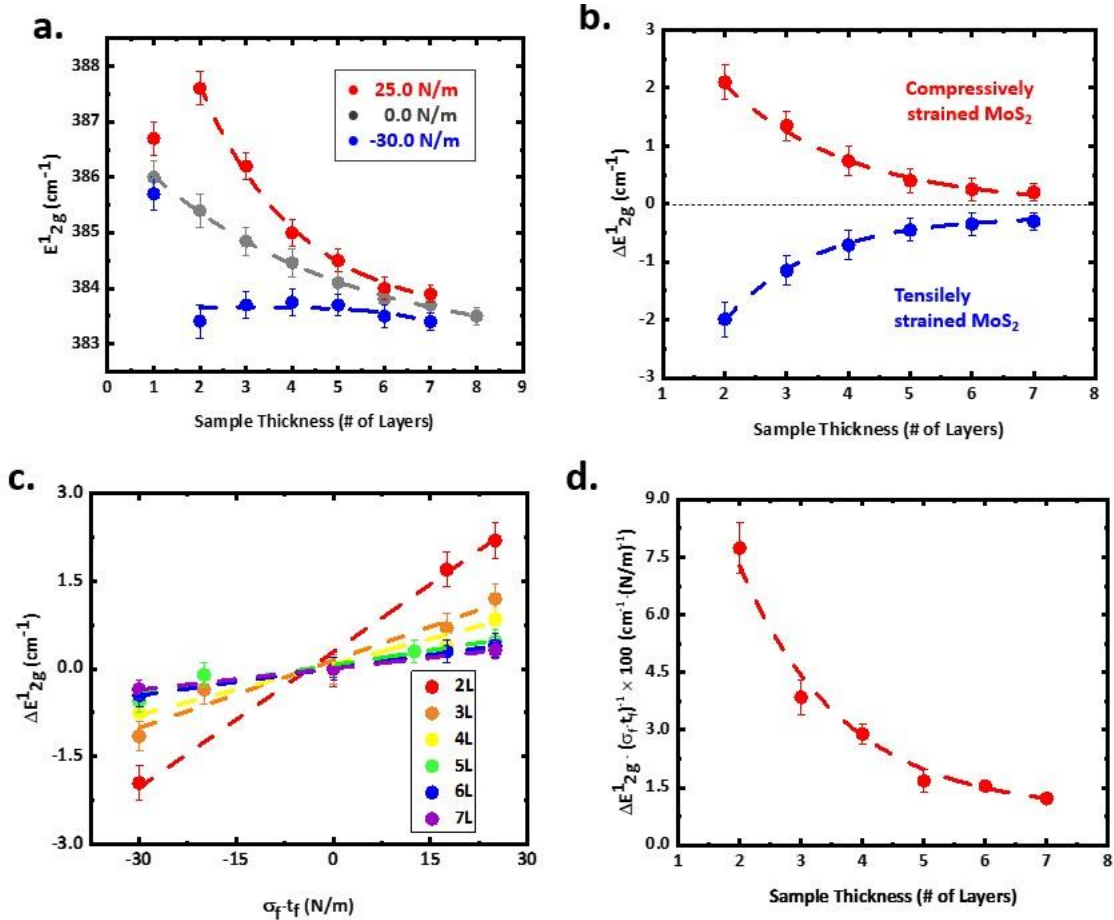


Figure 3: (a) Extracted E^{1}_{2g} peak positions varying with thickness and thin film stress for MoS₂ exfoliated on single-crystal MgO substrates. Red denotes tensile thin film stressor (MgF₂), grey is no stressor, then blue is a compressive thin film stressor (MgO). Dashed lines exhibit fitted exponentials to each curve for clarity. (b) Calculated E^{1}_{2g} peak shifts from (a). (c) Displayed is the E^{1}_{2g} peak shifts for each thickness sample with varying thin film force. The dashed lines are the fitted linear function for each layer. (d) The slope for each layer (determined from (c)) is then plotted and fit to an exponential decay function (dashed line).

upward peak shift within the E^{1}_{2g} mode distributed across the flake, revealing successful compressive strain induced from the tensile MgF₂ thin film stressor. Figure 2b presents a control (no encapsulation) 2L sample, here we can observe a negligible amount of strain

transferred from the exfoliation process and a $E^{1_{2g}}$ peak $\sim 2 \text{ cm}^{-1}$ lower than that of the encapsulated flake. The strain transferred into the MoS_2 samples are subjected to small amounts of variations (Figure 2a), which can be attributed from variables such as flake geometry, disparity of the TMDC's adhesion to the substrate, and etc.

2D Raman mappings were conducted for encapsulated and control flakes from 1L to 7L. Figure 3a shows the $E^{1_{2g}}$ peak shifts within the MoS_2 flakes with a tensile MgF_2 encapsulation (red), no encapsulation (grey), and a compressive MgO encapsulation (blue). From 2L to 7L, there exists an exponential decay to the control peak positions (Figure 3a). This dependence is clearly seen when observing the peak shifts in the encapsulated films from the starting value of 2 cm^{-1} (Figure 3b). Specifically in the monolayer samples, we observe very small peak shifts suggesting this layer is mostly fixed to the substrate. We then map the peak shifts for each thickness with varying thin film force (Figure 3c). The linear trend confirms strain transferred into the MoS_2 flakes originates from application of thin film force. Peak shift versus thin film force slopes are extracted for each thickness, again displaying an exponential dependence (Figure 3d). The exponential dependence is attributed from the overall Raman signal being the result of superimposed Raman signatures from each layer within a sample. In the case of a 2L sample, the top layer will be strained entirely by the stressor while the bottom layer is to a degree fixed to the substrate. Therefore, the measured Raman signal for the 2L sample is the coexistence of Raman signatures from the top strained layer and bottom partially fixed (very slight strain transfer) layer. We will combine these results with computational simulations to find out the actual strain distribution in the c-axis.

Atomistic modeling was carried out using the LAMMPS software package to study strain transfer on several MoS_2 structures with different number of layers.^{25,26} Crystal structure of MoS_2 is of a layered material with hexagonal coordination having A-B stacking sequence

between neighboring layers. Within each layer there are three sublayers of S-Mo-S atoms which results in each Mo atom being connected to six intralayer neighboring S atoms forming a trigonal prismatic geometry.²⁷ Intralayer atoms are connected by strong covalent bonds with lattice constant $a = 3.17 \text{ \AA}$, whereas interlayer atoms are connected by weak van der Waals interaction having lattice constant $c = 12.29 \text{ \AA}$ in the out-of-plane direction. A many-body reactive empirical bond-order (REBO) potential, parameterized for Mo-S systems, was used to model the covalent interactions and a two-body Lennard-Jones potential was used for interlayer van der Waals bonds.^{28,29} This specific potential has been widely reported to

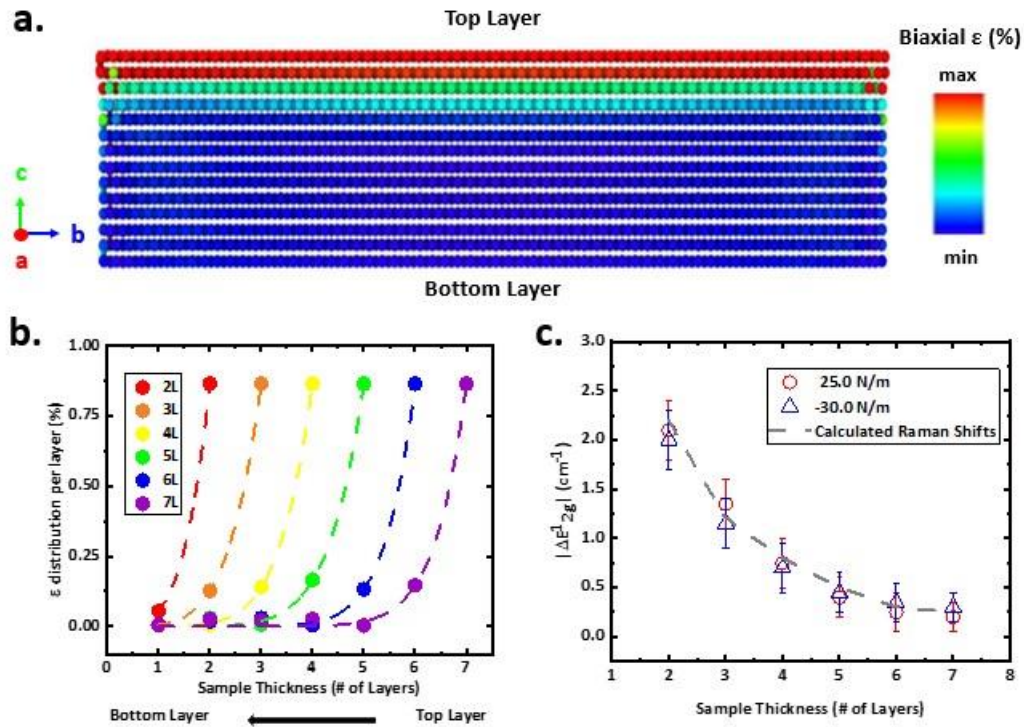


Figure 4: (a) Presents the strain distribution throughout a 7L sample of MoS₂ from MS simulations. Bottom layer is fixed, mimicking adhesion to the substrate. (b) Layer-by-layer strain distribution for various thickness samples determined from MS. (c) Presents calculated E_{12g}^1 peak shifts (grey line) compared to actual measured E_{12g}^1 peak shifts for both tensile and compressive thin film stressors.

accurately predict structural and mechanical properties, in addition to simulating structural phase transformations and complex mechanical loading (i.e. nanoindentation).^{30,31} Initial structures with almost square planar dimensions of 20 nm² were created, with each layer consisting of approximately 13,400 atoms and thickness was varied between 12.29 Å and 43 Å (corresponding to two to seven layers).

Initially, structures were relaxed using a conjugate gradient energy minimization algorithm to ensure minimum energy configurations. Subsequently, the molecular statics (MS) method was used (0 K) where a constant incremental biaxial strain in x and y direction was applied on the top layer of all the structures. Constant strain on the top layer was ensured by applying symmetric linearly varying displacement profile. Given our samples experimentally are fully encapsulated, we choose to mimic this in simulations with a biaxial strain distribution to replicate pulling in all directions. Biaxial strain was incremented by $\Delta = 0.14\%$ ($\epsilon = \sqrt{\epsilon_x^2 + \epsilon_y^2}$) up to final biaxial strain magnitude of $\epsilon = 0.85\%$. Between each increment, the atoms at the top layer were kept stationary and energy minimization was performed whereas the bottom layer was either kept fully fixed or fully free, forming two separate sets of results with distinct boundary conditions. None of the above boundary conditions alone are believed to represent the experimental conditions at the thin film-substrate interface due to unquantified compliance present at the interface. Therefore, a linear combination of the results from these two extreme cases was taken that best represents the experimental boundary condition at the substrate (estimated to be 75% fixed from Figure 3a). Free surface boundary in all directions was used to assist a heterogeneous strain transfer across layers. Finally, Ovito open visualization tool was used to visualize the atoms afterwards where atomic strains of all the atoms in a layer was used to compute the average strain of individual layers and subsequently for the whole structure.³² Using atomic strain provides the local strain information necessary for this kind of analysis and as shown in Figure 4a can capture the spatial information of local strain along the c-axis.³³ The strain

of individual layers was also independently estimated by the percentage change in length of each layer in planar (x-y) directions. Working with length change eliminates issues that may occur from the statistical nature of the atomic strain quantities.

Figure 4b shows the exact computationally simulated strain within each layer for 2L-7L samples. The 2L layer sample has 0.85% ϵ concentrated within the top layer, there is a small amount of strain transferred of 0.07% to the bottom layer for this sample since the bottom layer is predicted to be 75% fixed. For samples 3L-7L, the top layer has ϵ of 0.85% while the next layer decreases drastically to a ϵ of 0.12%, then the bottom layers have negligible amounts of strain. To directly compare what we see experimentally to the computational results, we first quantify translation factors to convert Raman peak shifts (cm^{-1} to ϵ (%)) (Figure S6). The overall Raman signature measured experimentally is a superposition of optical responses from each layer within the sample, similar to what is observed in Raman on TMDC heterostructures.^{34,35} We simulate the $E^{1_{2g}}$ Lorentzian responses from each layer (for 2L-7L samples), where the Lorentzian peak position of each layer is set to match the strain based off computational results. We superimpose the simulated responses from each layer for each sample thickness, then extract the peak position of the resulting Lorentzian response. Upon comparing the calculated peak shifts to that of our experimental results, we observe almost one-to-one matching between the measured peak shifts and our simulation (Figure 4c). Strain transferred into the first two layers matches the strain penetration regime observed in other works, where strain is induced into MoS_2 from silver nanoparticles.³⁶ At lower values of strain magnitude to the top layer, simulations predict that the c-axis strain transfer lengthscale may be increased due to decrease in interlayer slippage.

We have been able to show that with the employment of thin film stressors, we are able to strain engineer 2D MoS_2 . Within MoS_2 at this strain magnitude, the strain can penetrate two layers in the c-axis direction from the applied stress. The strain transfer lengthscale is likely unique to each 2D material depending on interlayer van der Waals coupling, with MoS_2

and graphene being close to the lower limit based on experimental and theoretical findings.³⁷ Our findings match with other experimental demonstrations that strain transfer is related to interlayer adhesion, the degree of strain transfer decay depends on the strength of the van der Waals bond.³⁸ Other TMDCs such as MoSe₂ and MoTe₂ have been predicted to have improved interlayer adhesion correlating with the size of the chalcogen, therefore they have a strong possibility of exhibiting longer strain penetration depths. When adopting strain engineering techniques from standard CMOS technology onto 2D TMDCs, we have shown that weak interlayer bonding significantly affects the strain transfer profile in the c-axis direction. Understanding these differences between 2D and 3D bonded systems opens the possibility to explore the unutilized strain degree of freedom in engineering 2D TMDC based devices. Previous attempts to strain these 2D TMDCs are typically macroscopic and require external mechanical forces, while our approach can be applied on-chip. Nanopatterning these thin film stressors may allow for engineering specific strain patterns within device structures, this is a technique that has been utilized heavily in 3D bonded Si transistors.³⁹ Static thin film stressors may also be combined with electric-field controllable dynamic strain from piezoelectrics to create gate-controllable changes in materials' properties. Our own work coupling thin film stress with dynamic strain from ferroelectric substrates has allowed for us to demonstrate a gate-controllable structural/electronic phase transition within MoTe₂.⁴⁰ Strain engineering can be a powerful tool that may open the possibility for control over a wide-variety of strain-tunable material properties in 2D TMDCs. By adapting popular strain engineering techniques from 3D-bonded industrial processes, these ideas may be adopted on the device scale to create new and otherwise unobtainable functionality in novel 2D devices.

Acknowledgment

This material is based upon work supported by the National Science Foundation (OMA1936250 and ECCS-1942815) and the National Science Foundation Graduate Research Fellowship Program (DGE-1939268). This work also made use of the Cornell Center for Materials Research Shared Facilities, which are supported through the NSF MRSEC programme (DMR-1719875).

Supporting Information Available

Presented after main text.

References

- (1) Qian, Z.; Jiao, L.; Xie, L. First-principles comparative study on the interlayer adhesion and shear strength of transition-metal dichalcogenides and graphene. *Chin. J. Chem.* **2020**, *38*, 753–760.
- (2) Akinwande, D.; Petrone, N.; Johnson, J. H. D. C.; Shi, L. Two-dimensional flexible nanoelectronics. *Nat. Commun.* **2014**, *5*, 5678.
- (3) Song, S.; Keum, D. H.; Cho, S.; Perello, D.; Kim, Y.; Lee, Y. H. Room Temperature Semiconductor–Metal Transition of MoTe₂ Thin Films Engineered by Strain. *Nano Lett.* **2016**, *16*, 188–193.
- (4) Desai, S. B.; Seol, G.; Kang, J. S.; Fang, H.; Battaglia, C.; Kapadia, R.; Ager, J. W.; Guo, J.; Javey, A. Strain-Induced Indirect to Direct Bandgap Transition in Multilayer WSe₂. *Nano. Lett.* **2014**, *14*, 4592–4597.

- (5) Guo, H.; Lu, N.; Wang, L.; Wu, X.; Zeng, X. C. Tuning Electronic and Magnetic Properties of Early Transition-Metal Dichalcogenides via Tensile Strain. *J. Phys. Chem. C*. **2014**, *118*, 7242–7249.
- (6) Liu, Y.; Li, Y. Y.; Rajput, S.; Gilks, D.; Lari, L.; Galindo, P. L.; Weinert, M.; Lazarov, V. K.; Li, L. Tuning Dirac states by strain in the topological insulator Bi₂Se₃. *Nat. Phys.* **2014**, *10*, 294–299.
- (7) Ge, Y.; Wan, W.; Yang, F.; Yao, Y. The strain effect on superconductivity in phosphorene: a first-principles prediction. *New. J. Phys.* **2015**, *17*, 35008.
- (8) O'Neill, A.; Olsen, S.; Escobedo-Cosin, E.; Varzgar, J.; Agaiby, R.; Chattopadhyay, S.; Dobrosz, P.; Bull, S. Strained silicon technology. *2006 8th Int. Conf. Solid-State Integr. Circuit Technol. Proc.* **2006**, 1–4.
- (9) Hoyt, J. L.; Nayfeh, H. M.; Eguchi, S.; Aberg, I.; Xia, G.; Drake, T.; Fitzgerald, E. A. Antoniadis, D. A. Strained silicon MOSFET technology. *Tech. Dig. - Int. Electron Devices Meet.* **2002**, 23–26.
- (10) Lloyd, D.; Liu, X.; Christopher, J. W.; Cantley, L.; Wadehra, A.; Kim, B. L.; Goldberg, B. B.; Swan, A. K.; Bunch, J. S. Band Gap Engineering with Ultralarge Biaxial Strains in Suspended Monolayer MoS₂. *Nano Lett.* **2016**, *16*, 5836–5841.
- (11) Nayak, A. P.; Bhattacharyya, S.; Zhu, J.; Liu, J.; Wu, X.; Pandey, T.; Jin, C.; Singh, A. K.; Akinwande, D.; Lin, J.-F. Pressure-induced semiconducting to metallic transition in multilayered molybdenum disulphide. *Nat. Commun.* **2014**, *5*, 3731.
- (12) Conley, H. J.; Wang, B.; Ziegler, J. I.; Richard F. Haglund, J.; Pantelides, S. T.; Bolotin, K. I. Bandgap Engineering of Strained Monolayer and Bilayer MoS₂. *Nano.Lett.* **2013**, *13*, 3626–3630.

- (13) Freund, L. B.; Suresh, S. Thin film materials: stress, defect formation and surface evolution. *Cambridge University Press 2004*, **2004**.
- (14) Ni, Z. H.; Wang, H. M.; Ma, Y.; Kasim, J.; Wu, Y. H.; Shen, Z. X. Tunable Stress and Controlled Thickness Modification in Graphene by Annealing. *Phys. Rev. B.* **2008**, *2*, 1033–1039.
- (15) Ennos, A. E. Stresses Developed in Optical Film Coatings. *Appl. Opt.* **1966**, *5*, 1.
- (16) Leplan, H.; Geenen, B. Residual stresses in evaporated silicon dioxide thin films: Correlation with deposition parameters and aging behavior. *J. Appl. Phys.* **1995**, *78*, 962.
- (17) Tamboli, S. H.; Puri, V.; Puri, R. K. Adhesion and stress of magnesium oxide thin films: Effect of thickness, oxidation temperature and duration. *Appl. Surf. Sci.* **2010**, *256*, 4582–4585.
- (18) Michail, A.; Delikoukos, N.; Parthenios, J.; Galiotis, C.; Papagelis, K. Optical detection of strain and doping inhomogeneities in single layer MoS₂. *Appl. Phys. Lett.* **2016**, *108*, 173102.
- (19) Li, S.; Miyazaki, H.; Song, H.; Kuramochi, H.; Nakaharai, S.; Tsukagoshi, K. Quantitative Raman Spectrum and Reliable Thickness Identification for Atomic Layers on Insulating Substrates. *ACS Nano.* **2012**, *6*, 7381–7388.
- (20) Li, H.; Wu, J.; Huang, X.; Lu, G.; Yang, J.; Lu, X.; Xiong, Q.; Zhang, H. Rapid and Reliable Thickness Identification of Two-Dimensional Nanosheets Using Optical Microscopy. *ACS Nano.* **2013**, *7*, 10344–10353.
- (21) Linn, J. H.; Swartz, W. E. An XPS study of the water adsorption/desorption characteristics of transition metal oxide surfaces: Microelectronic implications. *Appl. Surf. Sci.* **1984**, *20*, 154–166.

- (22) Blech, I.; Cohen, U. Effects of humidity on stress in thin silicon dioxide films. *J. Appl. Phys.* **1982**, *53*, 4202.
- (23) Thomas, M. E.; Hartnett, M. P.; McKay, J. E. The use of surface profilometers for the measurement of wafer curvature. *J. Vac. Sci. Technol. A Vacuum, Surfaces, Film*, **1988**, *6*, 2570–2571.
- (24) Zhang, Y.; Guo, H.; Sun, W.; Sun, H.; Ali, S.; Zhang, Z.; Saito, R.; Yang, T. Scaling law for strain dependence of Raman spectra in transition-metal dichalcogenides. *J. Raman Spectrosc.* **2020**, *51*, 1353–1361.
- (25) Plimpton, S. Fast parallel algorithms for short-range molecular dynamics. *J. Comput. Phys.* **1995**, *117*, 1–19.
- (26) <https://lammps.sandia.gov/>.
- (27) Farr, J. P. G. Molybdenum disulphide in lubrication. a review. *Wear.* **1975**, *35*, 1–22.
- (28) Liang, T.; Phillpot, S. R.; Sinnott, S. B. Parametrization of a reactive many-body potential for mo–s systems. *Phys. Rev. B.* **2009**, *79*, 245110.
- (29) Stewart, J. A.; Spearot, D. E. Atomistic simulations of nanoindentation on the basal plane of crystalline molybdenum disulfide (MoS₂). *Model. Simul. Mater. Sci. Eng.* **2013**, *21*, 045003.
- (30) Dang, K. Q.; Simpson, J. P.; Spearot, D. E. Phase transformation in mono-layer molybdenum disulphide (MoS₂) under tension predicted by molecular dynamics simulations. *Scr. Mater.* **2014**, *76*, 41–44.
- (31) Wang, W.; Li, L.; Yang, C.; Soler-Crespo, R. A.; Meng, Z.; Glin Li, M.; Zhang, X.; Keten, S.; Espinosa, H. D. Plasticity resulted from phase transformation for monolayer

- molybdenum disulfide film during nanoindentation simulations. *Nanotechnology*. **2017**, *28*, 164005.
- (32) Stukowski, A. Visualization and analysis of atomistic simulation data with ovito—the open visualization tool. *Model. Simul. Mater. Sci. Eng.* **2009**, *18*, 015012.
- (33) Shargh, A. K.; Abdolrahim, N. Molecular dynamics simulation of structural changes in single crystalline silicon nitride nanomembrane. *Ceram. Int.* **2019**, *45*, 23070–23077.
- (34) Nikama, R. D.; Sonawaned, P. A.; Sankar, R.; Chen, Y.-T. Epitaxial growth of vertically stacked p-MoS₂/n-MoS₂ heterostructures by chemical vapor deposition for light emitting devices. *Nano Energy*. **2017**, *32*, 454–462.
- (35) Pak, S. et al. Strain-Mediated Interlayer Coupling Effects on the Excitonic Behaviors in an Epitaxially Grown MoS₂/WS₂ van der Waals Heterobilayer. *Nano. Lett.* **2017**, *17*, 56345640.
- (36) Sun, Y.; Liu, K.; Hong, X.; Chen, M.; Kim, J.; Shi, S.; Wu, J.; Zettl, A.; Wang, F. Probing Local Strain at MX₂-Metal Boundaries with Surface Plasmon-Enhanced Raman Scattering. *Nano. Lett.* **2014**, *14*, 5329–5334.
- (37) Levita, G.; Molinari, E.; Polcar, T.; Righi, M. C. First-principles comparative study on the interlayer adhesion and shear strength of transition-metal dichalcogenides and graphene. *Phys. Rev. B.* **2015**, *92*, 085434.
- (38) Wang, R.; Lange, F. R. L.; Cecchi, S.; Hanke, M.; Wuttig, M.; Calarco, R. 2D or Not 2D: Strain Tuning in Weakly Coupled Heterostructures. *Adv. Funct. Mater.* **2018**, *28*, 1705901.

- (39) Jain, S. C.; Harker, A. H.; Atkinson, A.; Pinaridi, K. Edge-induced stress and strain in stripe films and substrates: A two-dimensional finite element calculation. *J. Appl. Phys.* **1995**, *30*, 1630.
- (40) Hou, W.; Azizimanesh, A.; Sewaket, A.; Peña, T.; Watson, C.; Liu, M.; Askari, H.; Wu, S. M. Strain-based room-temperature non-volatile MoTe₂ ferroelectric phase change transistor. *Nat. Nanotechnol.* **2019**, *14*, 668–673.

Supplementary Information:
Strain Engineering 2D MoS₂ with Thin Film
Stress Capping Layers

Tara Peña,^{*,†} Shoieb A. Chowdhury,[‡] Ahmad Azizimanesh,[†] Arfan Sewaket,[†]
Hesam Askari,[‡] and Stephen M. Wu^{†,¶}

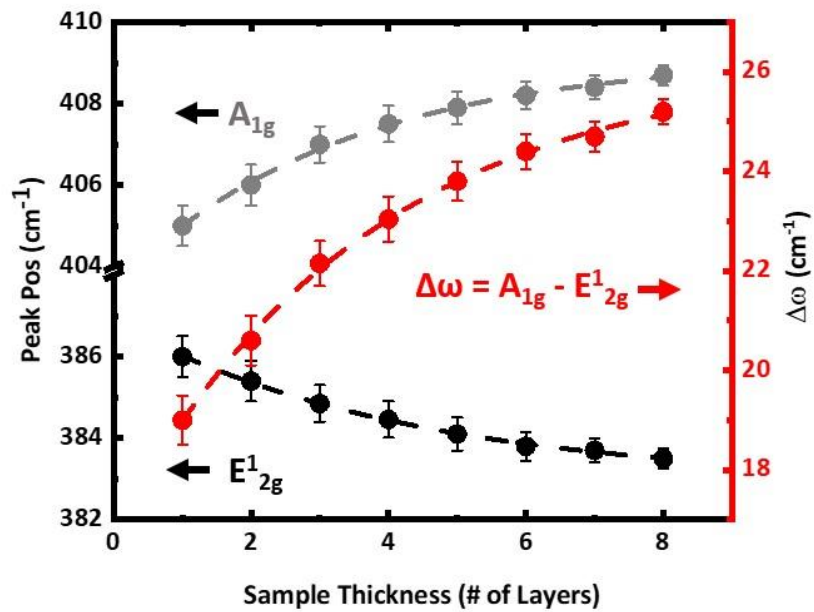
[†]*Department of Electrical & Computer Engineering, University of Rochester, Rochester,
NY, USA.*

[‡]*Department of Mechanical Engineering, University of Rochester, Rochester, NY, USA.*

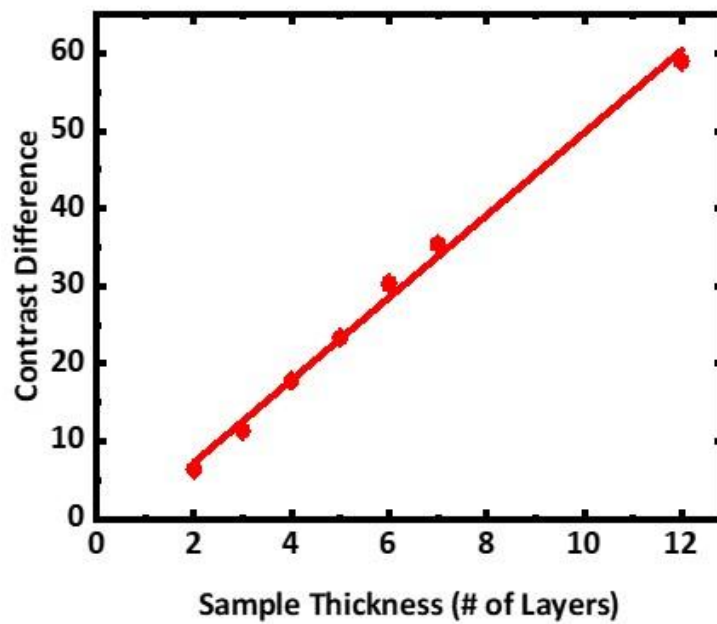
[¶]*Department of Physics & Astronomy, University of Rochester, Rochester, NY, USA.*

*E-mail: tpena@ur.rochester.edu

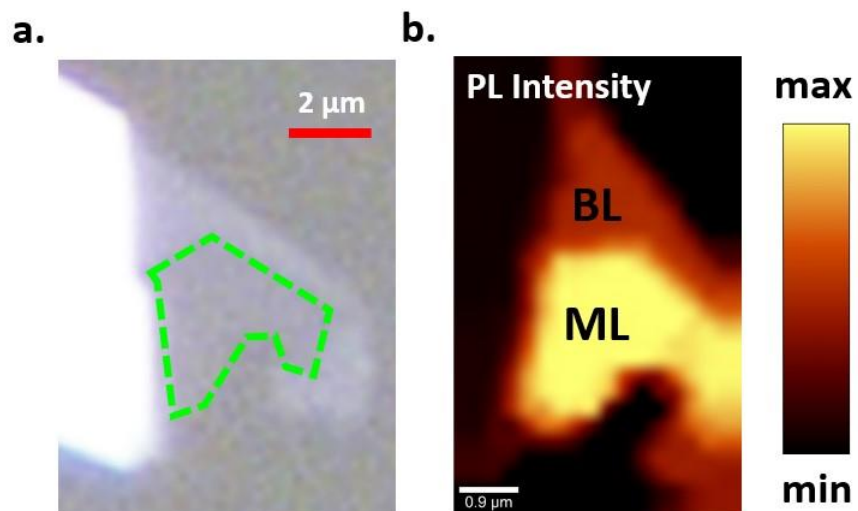
Layer Identification



Supplementary Figure 1: The in-plane (black) and out-of-plane (grey) Raman peak positions with respect to the number of layers for control MoS₂ on a single-crystal MgO substrate. Red curve denotes the difference between the two peaks.

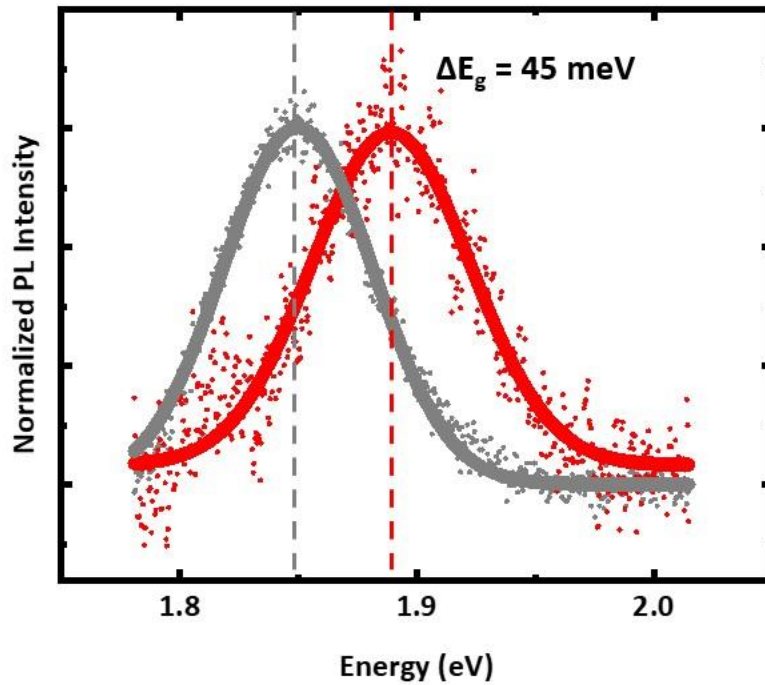


Supplementary Figure 2: Optical contrast difference between MoS₂ layers and single-crystal MgO substrates. Contrast values are determined from optical micrographs with same exposure.



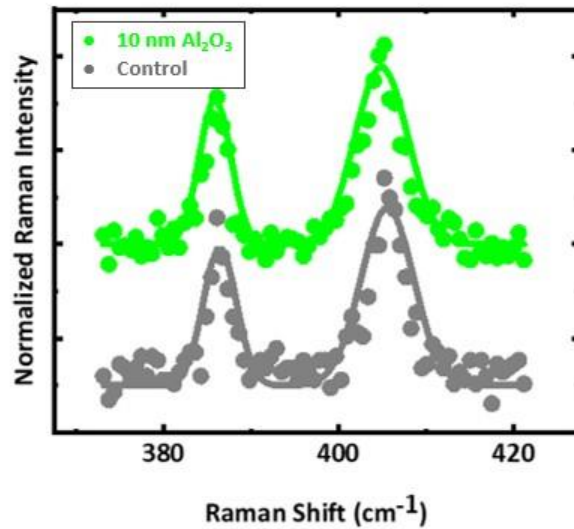
Supplementary Figure 3: (a) Control monolayer and bilayer (2L) MoS₂ optical micrograph, green dashed line outlines the monolayer region. (b) Photoluminescence (PL) intensity map of the same sample, confirmation of monolayer is made by the drastic increase of intensity and a bandgap of 1.85 eV.

Photoluminescence (PL) with Thin Film Force



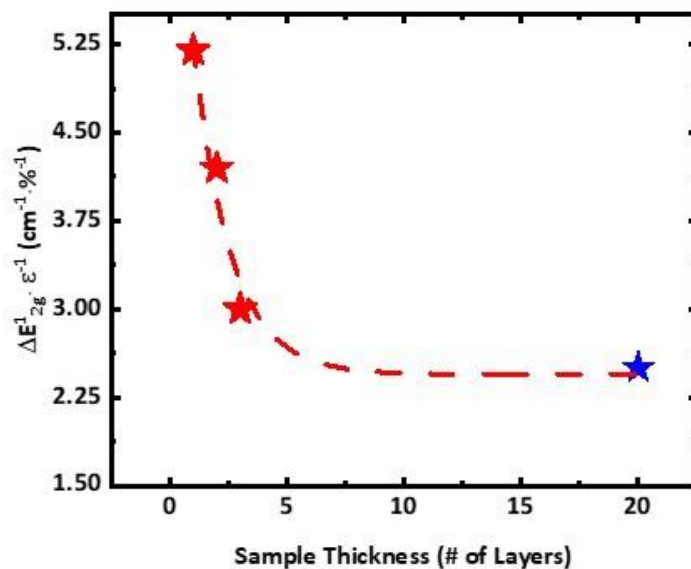
Supplementary Figure 4: Normalized PL intensity of control 2L MoS₂ (grey) and MgF₂ encapsulated (red) 2L MoS₂. There is a shift in the bandgap of about 45 meV, which is roughly expected from 0.5% biaxial compressive strain onto a 2L sample.¹

Contribution of 10 nm Al₂O₃ Adhesive Layer on 2L MoS₂



Supplementary Figure 5: Grey presents Raman spectra of a control 2L flake, while the green presents Raman spectra of a 2L encapsulated only in 10 nm Al₂O₃. Raw data is presented with dots while the Lorentz fit is presented with the solid line. It is unlikely the results from the main text are coming from the effects of the adhesive 10 nm Al₂O₃ layer alone, the E_{12g} and A_{1g} peak positions and FWHMs before and after deposition of the 10 nm Al₂O₃ are the same within experimental error.²

Converting Raman Peak Shifts to Strain



Supplementary Figure 6: For MoS₂ under biaxial in-plane strain, there are linear translation factors that relates E^{1_{2g}} peak shifts to strain magnitude. This translation value has been experimentally determined to vary with MoS₂ thickness. We estimate these factors from previous work implementing biaxial strain onto MoS₂. Red stars denote translation factors determined from previous biaxial strain work.¹ Blue star denotes translation factor value for bulk MoS₂.³ Dashed line represents exponential decay fit, extrapolating these values for layers 4-7.

References

- (1) Lloyd, D.; Liu, X.; Christopher, J. W.; Cantley, L.; Wadehra, A.; Kim, B. L.; Goldberg, B. B.; Swan, A. K.; Bunch, J. S. Band Gap Engineering with Ultralarge Biaxial Strains in Suspended Monolayer MoS₂. *Nano Lett.* **2016**, *16*, 5836–5841.
- (2) Michail, A.; Delikoukos, N.; Parthenios, J.; Galiotis, C.; Papagelis, K. Optical detection of strain and doping inhomogeneities in single layer MoS₂. *Appl. Phys. Lett.* **2016**, *108*, 173102.
- (3) Nayak, A. P.; Bhattacharyya, S.; Zhu, J.; Liu, J.; Wu, X.; Pandey, T.; Jin, C.; Singh, A. K.; Akinwande, D.; Lin, J.-F. Pressure-induced semiconducting to metallic transition in multilayered molybdenum disulphide. *Nat. Commun.* **2014**, *5*, 3731.